IEEE Access
Multidisciplinary | Rapid Review | Open Access Journal

Received 14 November 2023, accepted 8 December 2023, date of publication 13 December 2023,
date of current version 19 January 2024.

Digital Object Identifier 10.1109/ACCESS.2023.3342713

RESEARCH ARTICLE

Low Loss Wideband 4 × 4 Butler Matrix Networks Based on Substrate Integrated Waveguide for 5G Applications

YAQDHAN MAHMOOD HUSSEIN, MOHAMAD KAMAL A. RAHIM, (Senior Member, IEEE), NOOR ASNIZA MURAD, (Senior Member, IEEE), AND HATEM ODAY HANOOSH

Advance RF and Microwave Research Group (ARFMRG), Faculty of Electrical Engineering, Universiti Teknologi Malaysia (UTM), Johor Bahru, Johor 81310, Malaysia

Corresponding author: Yaqdhan Mahmood Hussein (yaqthanm79@gmail.com)

This work was supported by the Ministry of Higher Education (MOHE) under Fundamental Research Grant Scheme FRGS/1/2021/STG04/UTM/01/1 and grant 09G19 School of Postgraduate Studies (SPS), Research Management Centre, Advanced RF and Microwave Research Group, Faculty of Electrical Engineering, Universiti Teknologi Malaysia (UTM), Johor Bahru.

ABSTRACT Current wireless communications urgently need to provide huge data rates, high gain and high directivity radiation pattern beams. Therefore, beamforming networks (BFNs) are introduced to provide these needs. Butler matrix (BM) is a type of beamforming network, which can be realized using fixed network circuits and feeds the antenna array. BM at high frequency suffers from components loss and phase error for massive network, especially when it is implemented using common microstrip structures. Different transmission lines such as waveguide and substrate integrated waveguide (SIW) are studied and introduced to realize Butler matrix. SIW structures are good candidate for the implementation of BM due to its property of low loss transmission line which comprises of properties of microstrip and waveguide technology. However, SIW antennas and structures at millimeter waves have unwanted radiation loss coming from the vias holes. In addition, the vias separation distance is dependent on waveguide size, which leads to a more massive beamforming network at 26-GHz. Hence, this thesis is proposing a more size-friendly and optimal SIW antenna beamforming structure to reduce the vias loss and provides higher bandwidth and gain at 26 GHz. The BM components such as 3 dB coupler, 0 dB crossover, and 45-degree phase shifter are designed by implementing metallic vias determination method. Size and distance of vias are the most important factors in determining the coupling ratio and phase shifts at output ports. Hence, the coupler is designed with different vias width and distance to obtain the correct phase and coupling at output ports. Then, the designed coupler is cascaded to form a 0-dB crossover. The phase shifter is designed with alerting vias distance inside the coupling area of SIW structure. The last component in beamforming is the design of SIW slot antenna based on longitude slot distributions. All the components are integrated to form a 4 × 4 BM with four slot antennas attached to BM networks. Microtrip separation feedline used to for coupler, crossover, BM and BFN. The proposed designs are simulated using CST software and fabricated by PCB LPKF ProtoMat printer. The outcomes of wide bandwidth with more than 1-GHz and high directive gain of more than 10-dB for the beamforming network are achieved. The output power of the BM is between −6-dB to −8-dB at all four ports with phase difference error less than 5°. Four directive beams are achieved at beam scanning of −14°, −41°, 40°, and −14° at port 1 to port 4 respectively. Hence, this 4 × 4-BM with four slot antenna theses have introduced a successful design of an antenna beamforming network based on SIW technology with significant characteristics at 26-GHz.

INDEX TERMS 5G, Butler matrix, coupler, crossover, beamforming network (BFN), millimeter waves, wideband.

The associate editor coordinating the review of this manuscript and approving it for publication was Jjun Cheng.

I. INTRODUCTION

In the last decades, the required demands to increase the bandwidth, capacity, and receiving sensitivity towards cellular users are urgently addressed for wireless communication systems [1]. Basically, cellular mobile networks are implemented with electromagnetic fields that broadcasts over different frequency bands over air-medium [2]. As a results, it is needed to provide higher capacity and a higher bandwidth. This is lead to search alternative bands higher than sub-6 GHz. Hence, millimeter wave's band is proposed due to the benefits of providing hundreds of bandwidth compared to lower bands [3]. Compared to the fourth generation (4G) systems which works in lower band, fifth generation (5G) is meant to operate at high cellular standards and provides better coverage and capacity [4]. To be able for implementing these bands into real world, antenna array, phased beams switching, and beamforming networks are proposed [5], [6], [7], [8]. Generally, at higher frequency such as 26 GHz and 28 GHz, the 5G systems have assigned to be realized for base station applications [9]. Hence, beamforming networks are the most suitable technology to be implemented for the base station applications at those frequencies. Beamforming networks are well known in wireless communication fields in such of providing high-performance, state-of-the-art devices, which gives a major part for 5G networks to be combined with multi-antenna which bounces a companionable structure such as high gain, high directivity, high capacity, and high efficiency [7].

Beamforming networks can be comprehended by implementing fixed network circuits such as Butler matrix. The Butler matrix (BM) is a conventional feeding network which significantly attracts attention due to its easiness to form high beam signal with numerous phase shift properties at the output [7], [8]. The BM involves with three components of 3-dB coupler, 0 dB crossover, and 45- degree phase shifter. The 3-dB coupler is a four-port network filter with quarter-wavelength transmission line between two coupled ports which produces 90- or 180-degrees phase difference. Therefore, the total size of the coupler is essentially inversely proportional to the frequency in order to keep the quarter-wavelength line. At millimeter wave frequencies the size of 3 dB coupler is comparably very small due to the small wavelength which causes unwanted crosstalk between the coupler branches [9]. For example, a coupler is designed at 28 GHz using microstrip technology in [10]. The branch coupling distance between two sections are 1 mm which produces a high loss in the insertion loss and high phase error more than 10°. In case the coupler is integrated to form a crossover and later used in Butler matrix, more losses and phase errors are expected. Therefore, substrate integrated waveguide technology (SIW) is introduced to improve the performance and reduce the losses. The beamforming including the antenna is designed using SIW structure to overcome components losses and crosstalk where signals are confined within the vias walls of the SIW structure. Nevertheless, it is not easy to control the phase and the magnitude by using standard vias hole in SIW design [11], [12], [13], especially for 3-dB coupler and phase shifter. For instance, a coupler and beamforming network are designed with standard vias separation width using diameter less than half wavelength in [14], [15], and [16]. This leads to increases the loss inside the vias and increases the insertion loss of the coupler and the transmission coefficients at the Butler matrix beamforming network. Therefore, a vias variation with controlling the width of vias for area coupling control of the SIW structure is proposed in this work. This research contributes to control the signal to be confined between the vias and reduces the loss inside the vias. the coupling error and the phase errors are reduced by using this proposed technique.

Hence, this paper introduces a wideband BM realized by four couplers with vias separations and one crossover with two phase shifters at 26 GHz. Four slots' antennas are integrated with butler matrix to form a directive four beams. The rest of the paper is divided as follows: Section II introduces the BM components design and the integration of BM with antennas. Section III presents the obtained measured results. Section IV concludes the findings.

II. DESIGN OF 4 × 4 BUTLER MATRIX BEAMFORMING NETWORK

The topology of the proposed Butler matrix is shown in Fig. 1. In addition, table 1 present path of each ports. The BM consists of 4 couplers of 90° phase difference between the output ports, two phase-shifters that provide a phase shift of 45o, and a crossover to avoid the overlapping of signals at the crossing. As shown in Figure 2, the input ports are represented as Port-1 (P1), Port-2 (P2), Port-3 (P3), and Port-4 (P4) and the output ports are indicated as Port-5 (P5), Port-6 (P6), Port-7(P7), and Port-8 (P8). The proposed layout of the new BM is shown in Figure 2. The phase shift that will be defined for every output port on the basis of the input port excitation. It has four cases; when the signal is fed to Port 1(P1), the phase difference will be −45° between adjacent output ports. The phase difference between the adjacent output ports is +135o for the Port 2 (P2) excitation. For the third case, when the signal is fed to Port 3 (P3), the phase difference between the adjacent output ports would be −135°. The phase difference between the adjacent output ports is +45° for the Port 4 (P4) excitation. In designing a BM, three parameters are considered; insertion-loss, return-loss and isolation-loss. Insertion-loss defines how the input power is split between the output ports. All couplers have the same coupling ratio of C = 0.5 Hence, the coupling ratio of the couplers beside the Butler matrix outputs can be derived as follows [17].

$$at\ P5 : (1 - c_2) = \frac{1}{3} \tag{1}$$

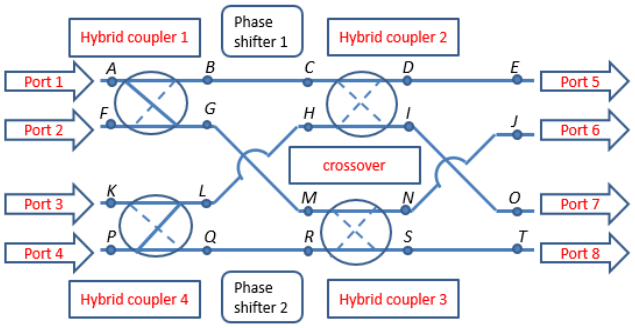

FIGURE 1. Topology of the proposed Butler matrix.

TABLE 1. Path of input ports into output ports with phase difference.

Excited Port	Path	Output Ports	Phase Difference
Port 1	A, B, C, D, E	5	-45°
	A, G, M, N, J	6	
	A, B, C, I, O	7	
	A, G, M, S, T	8	
Port 2	F, B, C, D, E	5	135°
	F, G, M, N, J	6	
	F, B, C, I, O	7	
	F, G, M, S, T	8	
Port 3	K, L, H, P, E	5	-135°
	K, Q, R, N, J	6	
	K, L, H, I, O	7	
	K, Q, R, S, T	8	
Port 4	P, L, H, D, E	5	45°
	P, Q, R, N, J	6	
	P, L, H, I, O	7	
	P, Q, R, S, T	8	

$$at\ P6 : C_2\,(1 - c_1) = \frac{1}{3} \tag{2}$$

$$at\ P7 : (C_1 \times C_2) = \frac{1}{3} \tag{3}$$

$$at\ P8 : (C_1 \times C_2) = \frac{1}{3} \tag{4}$$

The combination of coupler and crossover to construct the BM. The proposed coupler, crossover and BM were validated with the design specifications provided in Table 2. The detailed explanation and design of BM components are given below.

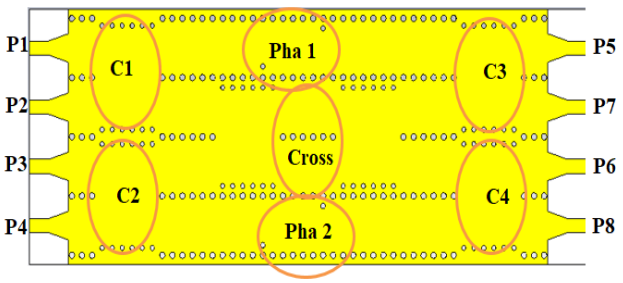

FIGURE 2. The proposed 4 × 4 Butler matrix.

TABLE 2. Design specification.

Parameters	Coupler	Crossover	Butler matrix
Operating Frequency	26 GHz	26 GHz	26 GHz
Required Bandwidth	>1 GHz	>1GHz	1 GHz
Phase difference	90°	0°	-45°, 135°, -135°, 45°.
Insertion loss	-3 ±2 dB	0 dB	-7 ±2 dB
Return loss	Below -10 dB	Below -10 dB	Below -10 dB
Isolation loss	Below -10 dB	Below -10 dB	Below -10 dB

A. BUTLER MATRIX COMPONENTS

Figure 3 shows the proposed 3 dB coupler based on vias separation. In order to prevent and to guide signal from leakage. The outputs of the coupler is coupled using vias metallic with cutting in the metal and substrate of electrical length of quarter wavelength($\lambda/4$) [18]. the two arrays of via hole were located on the adjacent wall of the coupler. The design of the SIW directional coupler consists of two perpendicular rectangular waveguides with a cross-region in which two metal posts were set symmetrically to control the signal. The two additional via posts placed in each port were used as a reflection cancelling element by varying sections of SIW. Port 1 is defined as an input port, Port 2 as the through port, Port 3 as a coupled port, and Port 4 as the isolated port. Step impedance is used as the transition between microstrip line and SIWs in order to physical match of electrical and magnetic fields distributions between the two media. Roger 5880 used as substrate with thickness 0.508mm and $\varepsilon r = 2.2$ with loss tangent 0.0009.

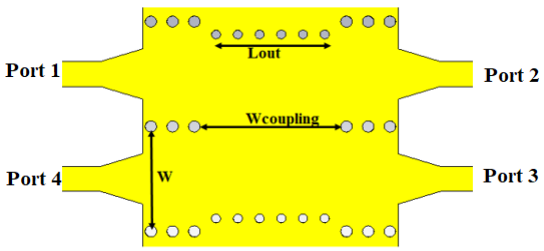

FIGURE 3. Structure of the proposed SIW coupler.

As in Figure 4(a), the width of the SIW vias (w) decreases, the resonance frequency tends to the desired frequency of 26 GHz. As well, the width of the coupling controls the output power at port 2 and port 3. Width of coupling calculated based on equation below [19]:

$$\Delta\varphi = (\beta 1 + \beta 2) \times wcoupling \tag{5}$$

where $\beta 1$ and $\beta 2$ are the propagation constant of TE10 and TE20 mode. $\Delta\,\varphi$ Value is $\pi/2$ need to satisfied the operation in this band. It tends to produce equal power of -3 dB coupling ratio as can see in figure 4 (b). As results, the dimension of the proposed coupler is selected as follows; the width of vias is set to 6.5 mm and the coupling area is set to be 11.5 mm.

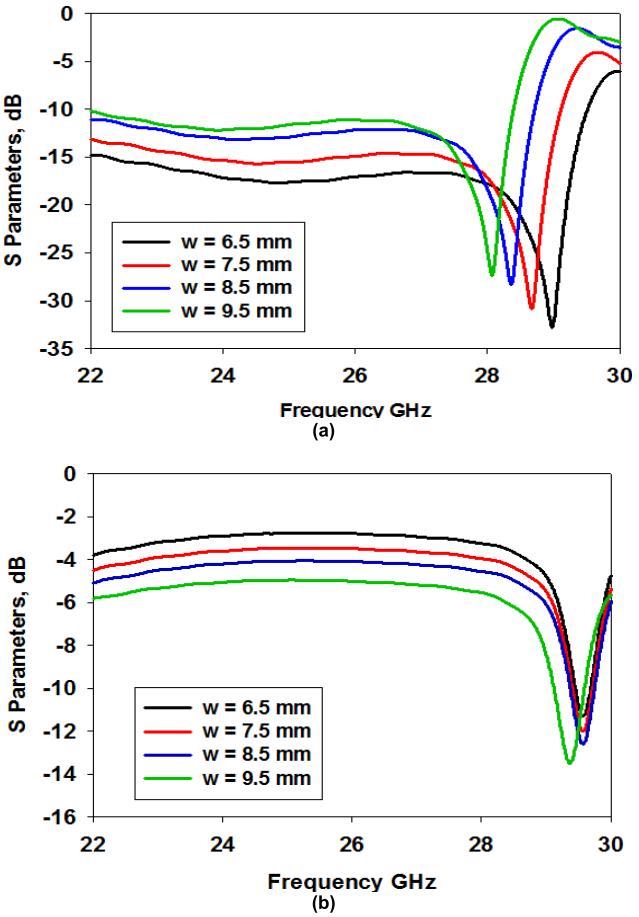

FIGURE 4. Simulated response. (a) Return loss, (b) output ports.

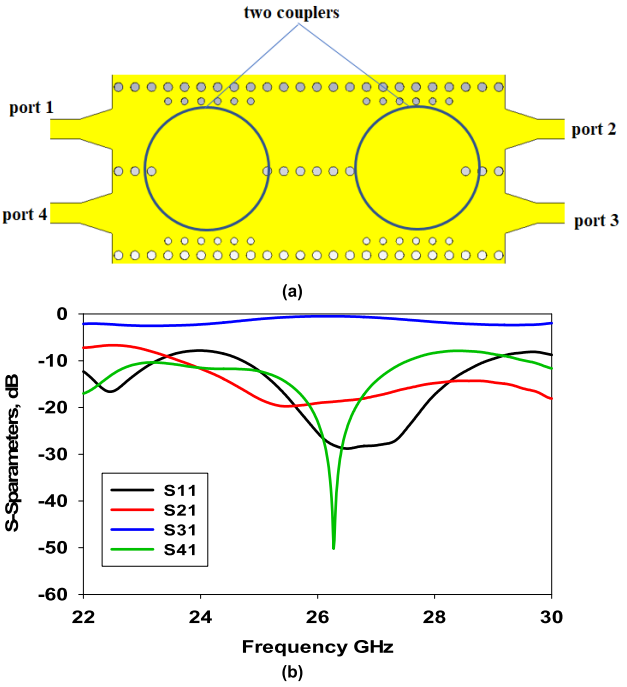

FIGURE 5. The proposed crossover and performance. (a) Crossover structure. (b) S-parameters.

The 0dB crossover is a four-port network with two input ports and two output ports named as port 1, port 4 and port 2, port 3 respectively. the crossover is designed by using SIW technology. From figure 4 the magnitude results it can be clearly seen that as the width of the SIW vias decreases, the resonance frequency tends to the desired frequency of 26 GHz. As well, the width of the coupling controls the output power at port 2 and port 3. It tends to produce equal power of −3 dB coupling ratio. As results, the dimension of the proposed coupler is selected as follows; the width of vias is set to 6.5 mm and the coupling area is set to be 11.5 mm. The crossover is normally designed by cascading two 3-dB coupler. The configuration of 0-dB crossover is illustrated in Figure 5 (a). The proposed crossover consists of two SIW couplers cascaded in series. Figure 5 (b) shows the performance of the crossover in terms of return loss and output power. When port 1 is excited, the return loss at 26 GHz is below −10 dB and the output is 0 dB at port 3. Both port 2 and port 4 are isolated with value less than −10 dB at desired frequency.

In order to maintain a correct phase difference at the Butler matrix output, a Schiffman phase shifter of two coupled transmission lines was designed as shown in Figure 6.

The widths of the Schiffman phase shifters, Wt. remain same as the widths of feeding transmission lines but the lengths of the Schiffman phase shifters, Ls are changing relative to the required phase values. The Schiffman phase shifters are realized by extending the corresponding lengths that are bent into arcs. The phase difference of the phase shifters can be determined by using Equation 6 [20]:

$$\textit{phase difference}, \Delta\emptyset = \frac{2\pi(Lm - Lr)}{\lambda g} \tag{6}$$

where *Lm, Lr* and are the main length, reference length and guide wavelength, accordingly. The main length, Lm and reference length, Lr are optimized to obtain the desired phase difference between the main line and the reference line which is at the first left output port of the proposed butler matrix. The designed phase shifters are combined with the couplers to analyses the performance results of the butler matrix. A cylindrical metal post, which is inserted in the SIW structure, is equivalent to a T-network and a phase shifter based on [21]. In the equivalent circuit of Figure 6, the capacitive coupling effect between the metal sides of the SIW and the cylindrical metal post is represented by two capacities while the mutual coupling effect between the top and bottom metal conductors is represented by an inductance. After design all components of butler matrix which is coupler crossover and phase shifter, next section will build fully butler matrix.

Figure 7 present structure of SIW. Figure 8 refers to the slot antenna design by using SIW technology with metallic vias at the left and right side of patch, the proposed design of antenna

sharing common ground plane to be directive antenna, All Dimensions of SIW Antenna presented in table 3. SIW design generally works in TE_{10} mode, m = 1, n = 0. Therefore, the equation for cutoff frequency is shown in equation 7:

$$fc = \frac{c}{2a} \tag{7}$$

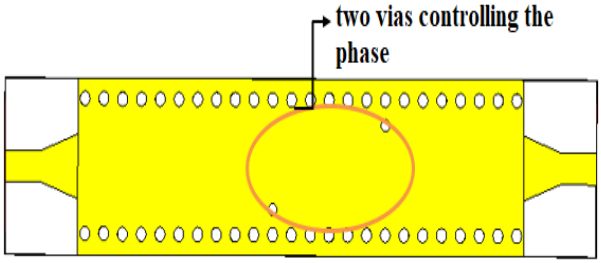

FIGURE 6. The proposed SIW phase shifter with two vias controllers.

where a is the total broad side dimension of the rectangular waveguide. Next, *ad* is the width of DFW (dielectric field waveguide) [22].

$$\text{ad} = \frac{\text{a}}{\sqrt{\varepsilon r}} \tag{8}$$

The design equations for SIW, which found by Wsiw is the separation between via rows (center to center).

$$Wsiw = ad + \frac{d^2}{0.95\ P} \tag{9}$$

Then, the equation for the separation distance "S" and diameter "D" control the radiation loss and return loss are as follows:

$$\lambda g = \frac{c}{f\sqrt{\varepsilon r}} \tag{10}$$

$$d \leq \frac{\lambda g}{5} \tag{11}$$

$$\text{P} \leq 2\text{d} \tag{12}$$

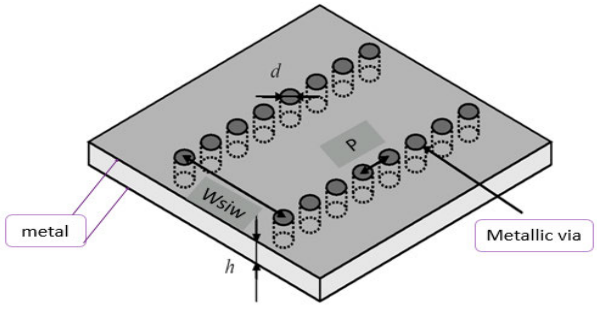

FIGURE 7. Configuration of an SIW structure synthesized using metallic via-hole arrays [23].

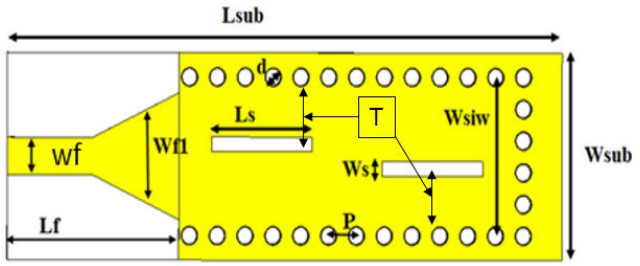

FIGURE 8. The proposed antenna with two slots.

TABLE 3. All dimensions of SIW antenna.

Definition	Parameters	Value (mm)
Substrate width	W_{sub}	8.5
Substrate Length	L_{sub}	25.9
Width of the slot patch	*Ws*	0.6
Length of the slot	L_s	4.7
Width of feed	W_f	1.556
Length of feed	L_f	8
Width of feeder SIW	*Wf1*	5.2
Length of patch	L_p	25
Diameter of vias	*d*	0.73
Separation between two vias	*P*	0.98
SIW vias width	*Wsiw*	5.5
Thickness of substrate	*h*	0.508
distance from the centre of slot to the edge of SIW vias	T	2.3

B. INTEGRATION OF 4 × 4 BM

The feedline of the proposed BM in figure 2 has been modified, the feedline of input and output ports separated by microstrip feedline as can in figure 9 reangling the feedlines of port 1, 4, 5 and 8 by 90 degree and each adjacent feedline ports 2, 3, 6 and 7 to be able solder SMA for each port. Figure 9 shows the integration of a 4 × 4 Butler matrix by constructing four couplers, one crossover, and two-phase shifters. To verify the concept of the 4 × 4 Butler matrix, a simulation process was performed using a Computer Simulation Technology (CST) software. The S-parameters response of return loss, isolation, and transmission coefficients are plotted for each input ports.

This section discusses S-parameters results as simulation in terms of return-loss and insertion-loss. For setup, Port-1 (P1) is fed with the signal while keeping all the other terminated using 50ohm loads. The results are summarized in Figure 10, and it can be observed that the simulated insertion-loss at Ports 5-8 is coming out to be -7 ± 2 dB, respectively which shows that the output ports power division in the BM network is approximately equal. Similarly, the simulated return-loss value is below -16 dB, which refers to good performance characteristics. All the simulated responses are taken between the frequency range of 24-28 GHz, respectively. It can also be observed from Figure 10 that at 26GHz frequency band 15%.

Figure 11 discusses the simulated S-parameters results in terms of return-loss and insertion-loss for Port-2 (P2) excitation. the Port-2 is fed with a signal while keeping all the

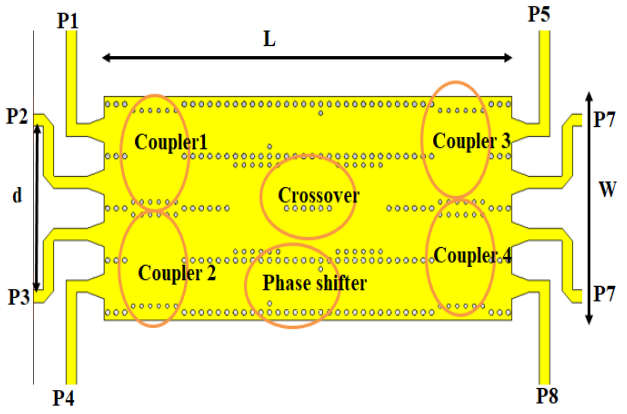

FIGURE 9. The proposed 4 × 4 Butler matrix.

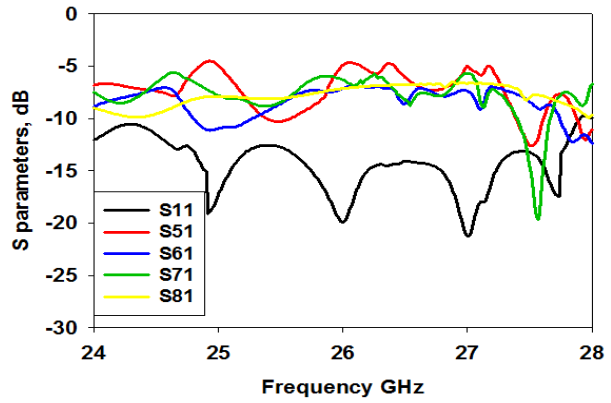

FIGURE 10. S-parameters simulated responses of the proposed Butler matrix at port 1 excitation.

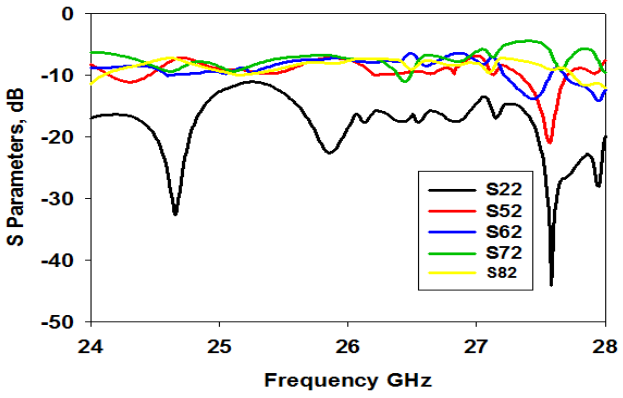

FIGURE 11. S-parameters simulated responses of the proposed Butler matrix at port 2 excitation.

other terminated using 50ohm loads. From 24GHz to 28GHz frequency range, the results in Figure 11 illustrate that the simulated return-loss is below −22 dB, and insertion-loss obtained at Port 5-8 is −7 ± 2 dB, respectively. According to the insertion-loss result observed in Figure 11, power division between the BM four output ports are approximately equal.

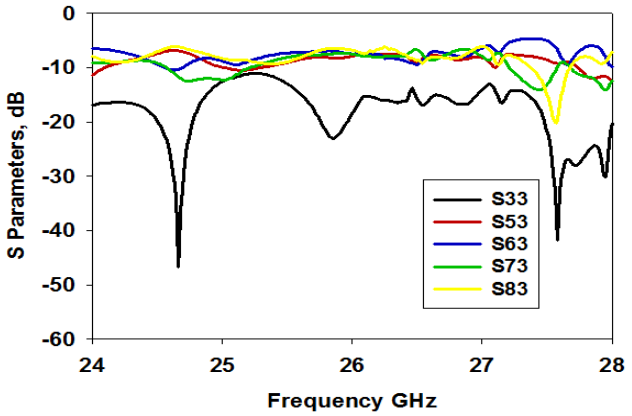

FIGURE 12. S-parameters simulated responses of the proposed Butler matrix at port 3 excitation.

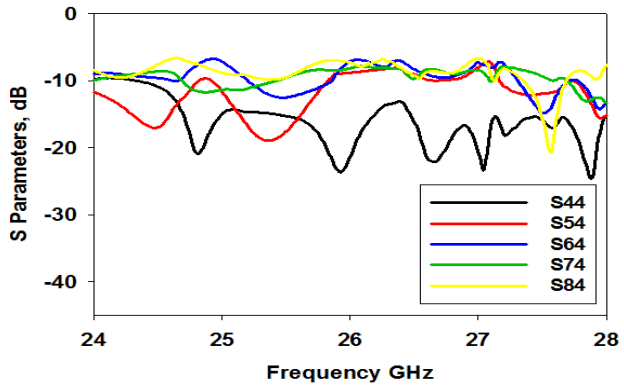

FIGURE 13. S-parameters simulated responses of the proposed Butler matrix at port 4 excitation.

Figure 12 discusses the simulated S-parameters results in terms of return-loss and insertion-loss for Port-3 (P3) excitation. Port-3 is fed with a signal while keeping all the other terminated using 50ohm loads. The results are summarized in Figure 12, and it can be observed that simulated insertion-loss at Ports 5-8 is coming out to be −7 ± 2 dB, respectively which shows that output ports power division in the BM network is approximately equal. Similarly, the simulated return-loss value is below −19 dB, which refers to good performance characteristics. All the simulated responses are taken between the frequency range of 24-28 GHz, respectively. It can also be observed from Figure 12 that at 26 GHz frequency band 15%.

Figure 13 discusses the simulated S-parameters results in terms of return-loss and insertion-loss for Port-4 (P4) excitation. Port-4 is fed with a signal while keeping all the other terminated using 50ohm loads. From 24GHz to 28GHz frequency range, the results illustrate that the simulated return-loss is below −14 dB and insertion-loss observed at port 5-8 is −7 ± 2 dB. According to the insertion loss result observed in Figure 13, the power division between the BM four output ports are approximately equal.

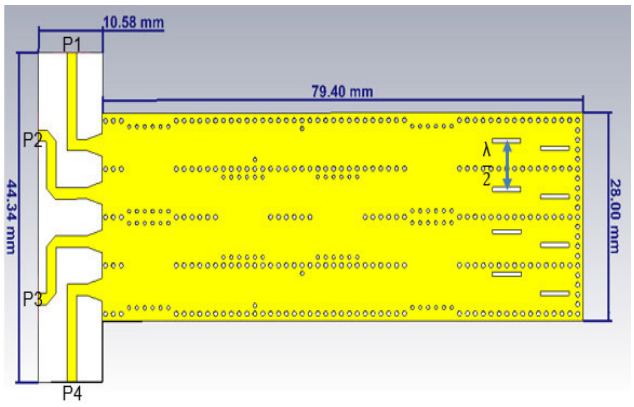

FIGURE 14. The antenna beamforming design using Butler matrix network with four SIW slot antennas.

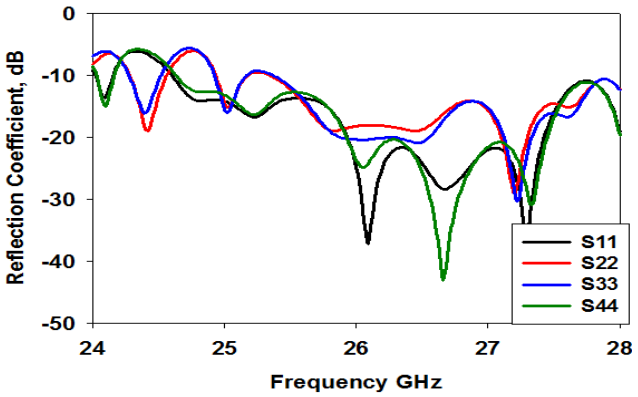

FIGURE 15. The simulated input powers of the proposed beamforming networks.

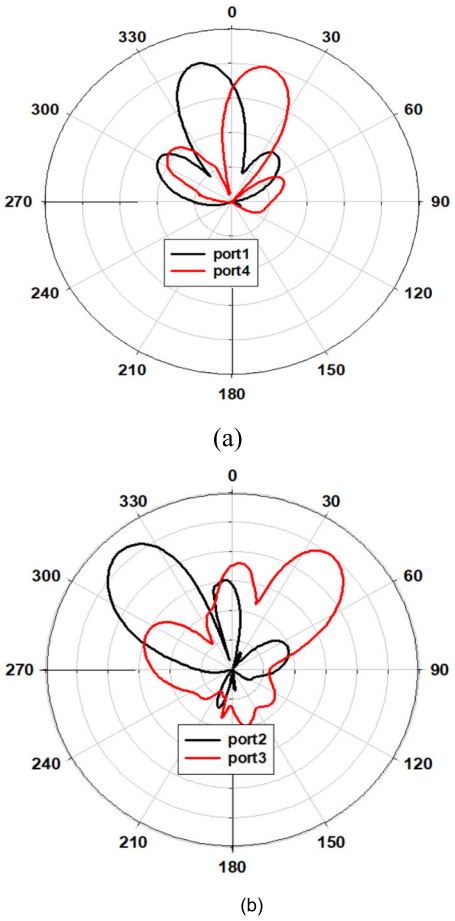

FIGURE 16. The performance of the proposed simulation antenna beamforming of radiation pattern at all ports.

C. ANTENNA BEAMFORMING BASED-BUTLER MATRIX

Figure 14 shows the integration of the proposed 4 × 4 Butler matrix with four slot SIW antennas at 26 GHz. The antennas are attached to the Butler matrix outputs with distance of a quarter wavelength (λ/4). The SIW antenna is essentially a standard slot antenna designed at 26 GHz to prove the concept of the Butler matrix beamforming network, the distance between two slots is (λ/2). A simulation response in terms of return loss and isolation are presented in Figure 15.

The microstrip straight feedline of BFN has been modified by separating each adjacent port as can be seen in Figure 14 to achieve enough distance between in ports to be able to solder SMA for BFN. The simulated results of the reflection coefficients of the BFN with microstrip separation feedline are shown in Figure 14. The reflection coefficients, S11 = −37 and S44 = −22dB, and the reflection coefficients, S22 and S33 = −20 dB and −17 dB which means a good return loss is obtained greater than 10 dB at the desired frequency with a wider bandwidth of almost 4 GHz as can be seen in figure 15.

The simulated radiation pattern results of the linear 1 × 4 antenna array with spacing 0.5λ and microstrip separation feedline are shown in Figure 14. Figure 18. shows the simulated results of the radiation pattern when Port-1(P1) or Port-2(P2) or Port-3(P3) or Port-4(P4) of the BM is excited. we are discussing the simulation results of BFN with microstrip separation feedline and d = 0.5λ at 26 GHz. When P1 and P4 are excited, a gain of 9.5 dB and 7.6dB is achieved, respectively. Although the gain 11.9 dB and 8.1 dB for P2 and P3 excitation, respectively. However, according to which the input port is excited, the peak of the beam rotates. the gain of BFN with a microstrip separation feedline achieved almost similar results to the BFN with a microstrip straight feedline according to gain and reflection coefficients has a bit loss come from the length of the microstrip separation feedline.

As seen in Figure 16(a), when input port P1 is fed with a signal, the main beam is directed to −14°. Meanwhile, the direction of maximum radiation is attained at −41°, as the signal is fed into input port P2. In Figure 16(b), for the input port P3 excitation, the main beam steers to +40°. When the input port P4 is excited, the direction of the main beam alters to +14°. when the input port P1 and P4 is excited, the half power beam width (HPBW) of the main

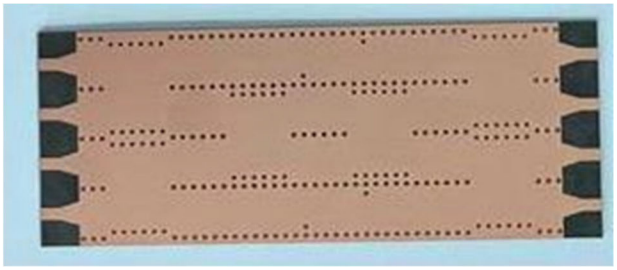

FIGURE 17. Roger substrate based fabricated prototype of the proposed 4 × 4 BM without microstrip separation feedline.

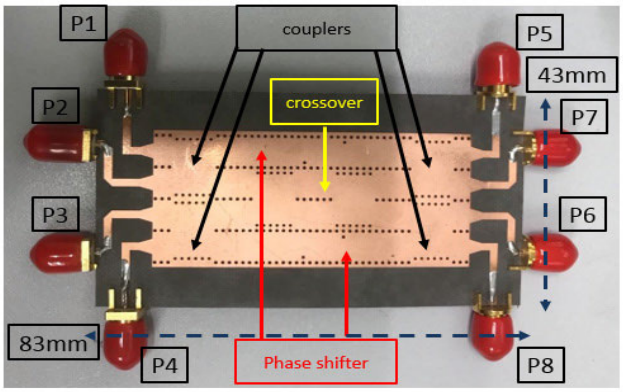

FIGURE 18. Fabrication of 4 × 4 Butler matrix.

lobe is 30° and 29.5°, respectively. Similarly, the HPBW is 32.5° and 32° for the excitation of input ports P2 and P3, respectively.

III. RESULTS AND DISCUSSIONS

The proposed 4 × 4 Butler matrix and antenna beamforming network are fabricated using Roger 5880 substrate with thickness of 0.508 mm and permittivity of $\varepsilon_r = 2.2$. The measurements in terms of S-parameters are performed using vector network analyser (VNA) with two cables and six termination dummy loads.

A. BUTLER MATRIX RESULTS

The feedline of the SIW butler matrix in Figure 17 has been modified, by separating all input and output ports to be able to solder SMA for each port. The BM was fabricated by integrating BLCs, crossover, and phase-shifter on a single roger substrate allowing them to share a common ground as illustrated in Figure 18. This is to develop a more compact and precise BM structure for the deployment in 5G SAA systems. Figure 18 indicates the overall area of the BM design to be without separation feedline 28 × 59 mm^2 while BM with separation 89 × 28 mm^2.

The design and fabrication of both 4 × 4 configuration of BM structure shown in Figures 17-18 indicate good agreement between the simulation results and measurement results of BM in Figure 18, although BM structure is not able to be measured (Figure 17) because of the distance between each adjacent port. From this point onwards, this thesis's discussion will be related to the 4 × 4 configuration of the BM structure as depicted in Figure 18. It can be seen from Figure 5.3 that when the signal is fed to P1-P4 (input ports), it can be transmitted to P5-P8 (output ports) with equally divided amplitude and predefined phase shifts as shown in TABLE 1.

This section discusses the measured S-parameters results in terms of return-loss and insertion-loss based on measured. For measurement setup, Port-1 (P1) is fed with the signal while keeping all the other terminated using 50ohm loads. The results are summarized in Figure 19 (a), and it can be observed that measured insertion-loss at Ports 5-8 is coming out to be −7 ± 2 dB, respectively which shows that the output ports power division in the BM network is approximately equal. Similarly, measured return-loss value is below −16dB, which refers to good performance characteristics. measured responses are taken between the frequency range of 24-28 GHz, respectively. It can also be observed from Figure 19 (a) that at 26GHz frequency band, the measured return-loss and average insertion-loss (S15, S16, S17, S18) is −20 dB and −7dB, respectively.

Figure 19(b) discusses the measured S-parameters results in terms of return-loss and insertion-loss for Port-2 (P2) excitation. For the measurement setup, the Port-2 is fed with a signal while keeping all the other terminated using 50ohm loads. From 24 GHz to 28 GHz frequency range, the results in Figure 19 (b) illustrate that the measured return-loss is below −22 dB, and insertion-loss obtained at Port 5-8 is −7 ± 2 dB, respectively. According to the insertion-loss result observed in Figure 19 (b), the power division between the BM four output ports are approximately equal. The measured return-loss is −19dB and the average insertion-loss (S25, S26, S27, S28) is −7 dB at 26GHz frequency band. When the signal is fed to Port-2, the results in Figure 19(b) are in good agreement with each other, indicating excellent BM performance.

Figure 19(c) discusses the measured S-parameters results in terms of return-loss and insertion-loss for Port-3 (P3) excitation. For the measurement setup, Port-3 is fed with a signal while keeping all the other terminated using 50 ohm loads. The results are summarized in Figure 19(c), and it can be observed that measured insertion-loss at Ports 5-8 is coming out to be −7 ± 2 dB, respectively which shows that output ports power division in the BM network is approximately equal. Similarly, the measured return-loss value is below −19 dB, which refers to good performance characteristics. All the measured responses are taken between the frequency range of 24-28GHz, respectively. It can also be observed from Figure 19 (c) that at 26GHz frequency band, the measured return-loss and average insertion-loss (S15, S16, S17, S18) is −16 dB and −7.7 dB, respectively. The measured and simulated results are in good agreement with each other, indicating excellent BM performance.

Figure 19(d) discusses the measured S-parameters results in terms of return-loss and insertion-loss for Port-4 (P4) excitation. For the measurement setup, Port-4 is fed with a

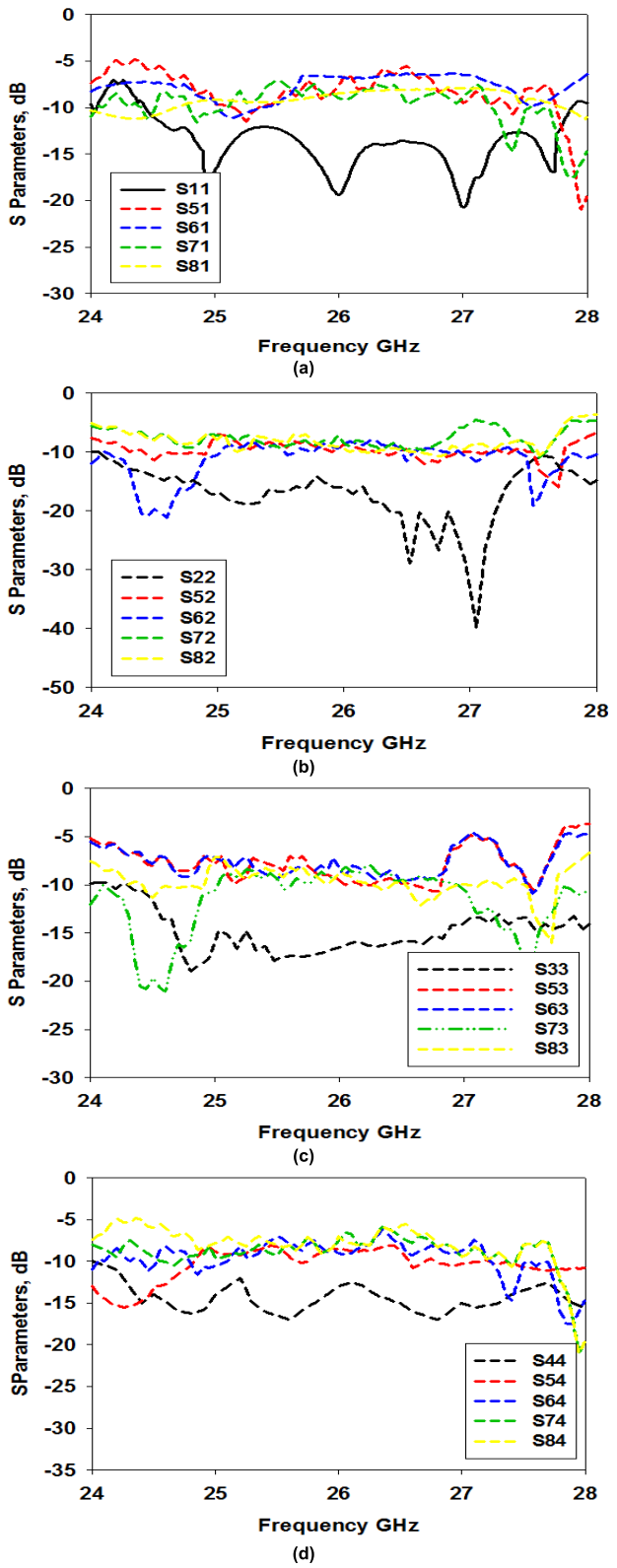

FIGURE 19. The measured performance of the printed 4 × 4 Butler matrix. (a) Port 1. (b) Port 2. (c) Port 3. (d) Port 4.

signal while keeping all the other terminated using 50ohm loads. From 24 GHz to 28 GHz frequency range, the results illustrate that the measured return-loss is below −14 dB and insertion-loss observed at port 5-8 is -7 ± 2 dB. According to the insertion loss result observed in Figure 19 (d), the power division between the BM four output ports are approximately equal. The measured return-loss is −14dB and the average insertion-loss (S45, S46, S47, S48) is −6.75 dB at 26 GHz frequency band. When a signal is fed to Port-4, the results in Figure 19 (d) show that they are in good agreement with each other, indicating excellent BM performance.

In this section, summaries result the phase difference of the proposed design BM between adjacent output ports. The phase difference is calculated by subtracting the phase from one output port to another. Figure 20 presents, the output signal to the simulated and measured BM phase difference between adjacent output ports when port-1 is excited. The result in Figure 20 illustrates good agreement between simulated and measured phase difference.

So, for the port −1 excitation of the proposed BM design in this paper, shows in Figure 20(a) the differences result between simulated and measured of the phase differences at center frequency 26 GHz of the BM. According to the simulated, the phase differences for output at P1 −45 is (S61-S51), (S71, S61), (S81-S71) −47.7°, −41°, and −43.5°. Is achieved between output ports P-5/P-6, P-6/P-7 and P-7/P-8, respectively. It can be noted from the simulated phase difference values that the error is 2.7°, 4° and 2°, respectively. The average phase was 43.9 and phase error of average phase is 1.1° shows in Figure 20(c).

Correspondingly, the measured phase differences present in figure 20(b), was (S61-S51), (S71, S61), (S81-S71) −50°, −40° and −41°, is achieved between output ports P-5/P-6, P-6 / P-7, and P-7/P-8, respectively, when the signal is fed to Port-1. It is important to note here that from the measured phase difference values, the error is 5°, 5° and 4°, respectively. The average phase difference was −42.9° and error of average is 2.1°. as can see in figure 20(c).

Figure 21 (a-b-c) shows the simulated and measured phase difference between the adjacent output ports of the BM for the excitation of Port-2. According to the design criteria listed in Table 1, which suggests +135° phase difference between the adjacent output ports. For the excitation of Port-2, the simulated phase differences achieved between the output ports are 138°, 139°, 130°, respectively, at 26GHz. The simulated phase difference values fluctuate from the target value of +135° by 3°, 4° and 5°, respectively. The average phase difference was 135.6° and phase error of average is 0.6°.

For the excitation of Port-2, the measured phase differences achieved between the output ports are 140°, 139° and 130°, respectively, at 26 GHz. It is important to note here that from the measured phase difference values, the error is 5°, 4° and 5°, respectively, which led to an average phase difference 136.3° error of 1.3°.

Figure 22 (a-b-c) illustrates the simulated and measured phase difference between the adjacent output ports of the BM when Port-3 is excited. The BM design specifications are given in Table 1, which suggests −135° phase difference

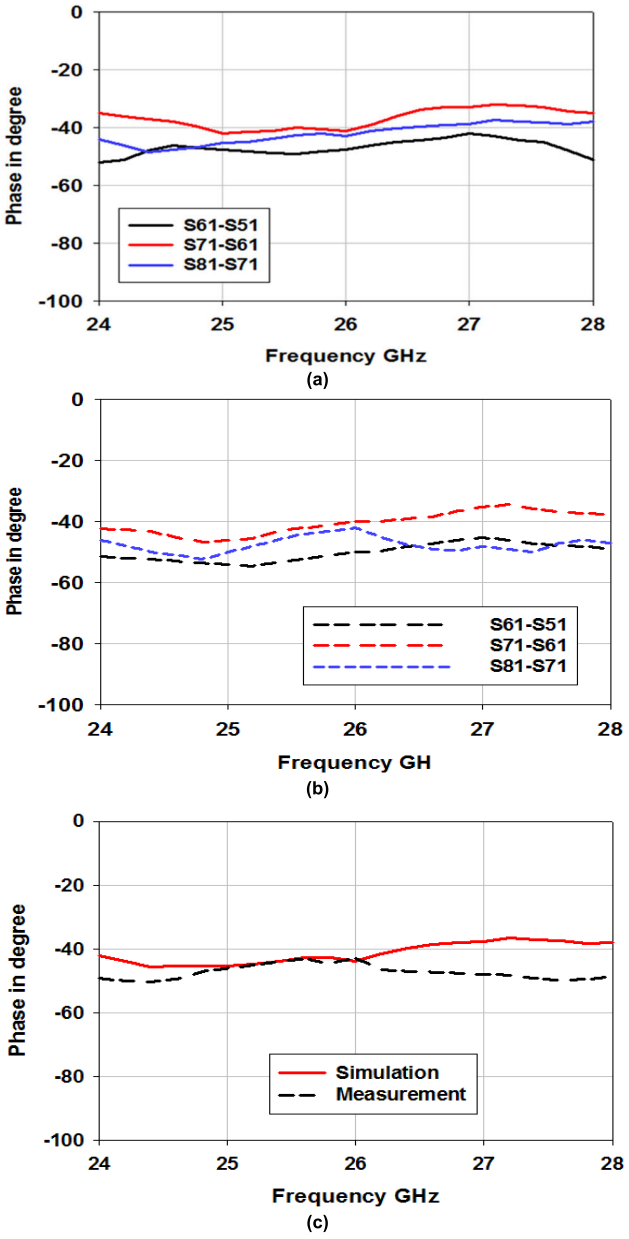

FIGURE 20. Phase shift at the output ports for the Port-1 excitation (a) Simulated, (b) Measured response, (c) Average phase differences.

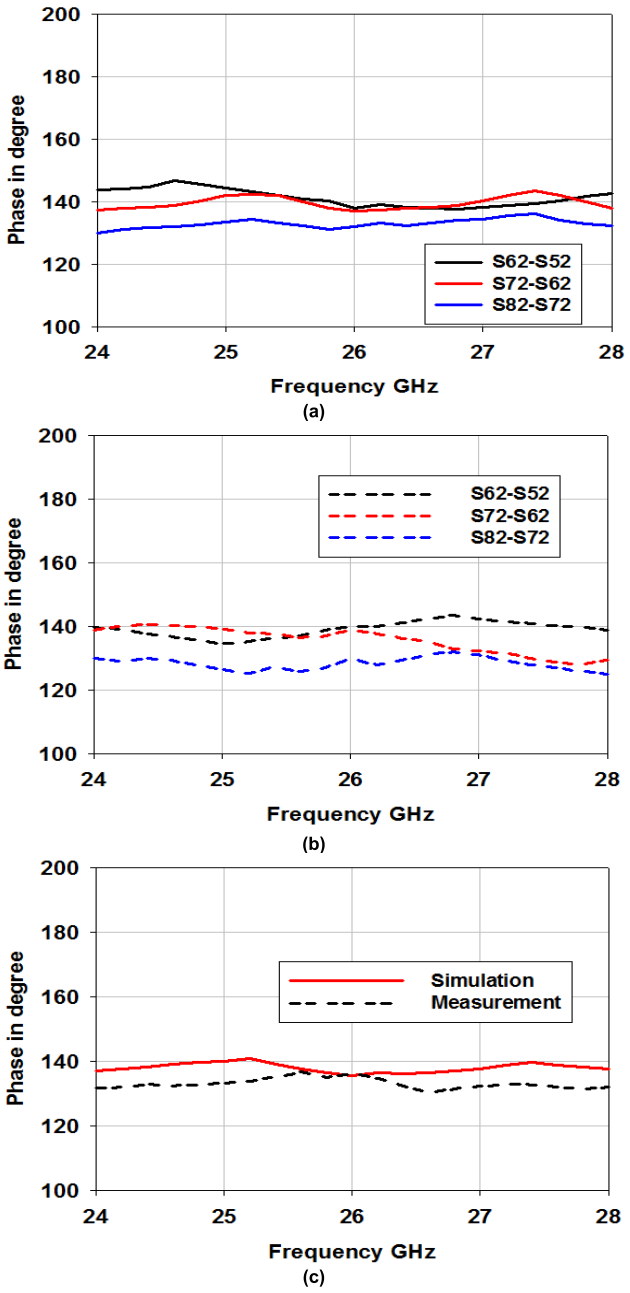

FIGURE 21. Phase shift at the output ports for the Port-2 excitation (a) Simulated, (b) Measured response, (c) Average phase differences.

between the adjacent output ports for the excitation of Port-3. So, for the Port-3 excitation of the proposed BM design in this thesis, the simulated phase differences (S63-S53) / (S73-S63) / (S83-S73) of −132.5° / −138° / −140° is achieved between Port-5 / Port-6, between port-6 / Port-7, and between Port-7 / port-8, respectively. It can be noted from the simulated phase difference values that the error is 2.5°, 3° and 5°, respectively. The average phase difference was 136.8 and phase error is 1.8°.

For the phase difference measurement results, the measured (S63-S53) / (S73-S63) / (S83-S73) phase difference of −131° / −140° / −142° is achieved between Port-5 / Port-6, between Port-6 / Port-7 and between Port-7 / Port-8, respectively, when the signal was fed to Port-3. It is important to note here that from the measured phase difference values, the error is 4°, 5° and 7°, respectively. The average phase difference was 137.6 and error is 2,6°.

Figure 23 (a-b-c) illustrates the simulated and measured phase difference between the adjacent output ports of the BM, when a signal is fed to Port-4. According to the design criteria listed in Table 1, it is suggested that the phase difference between the adjacent output ports to be +45°. For the excitation of Port-4, the simulated phase differences achieved between the output ports are 40°, 43°, 48°, respectively,

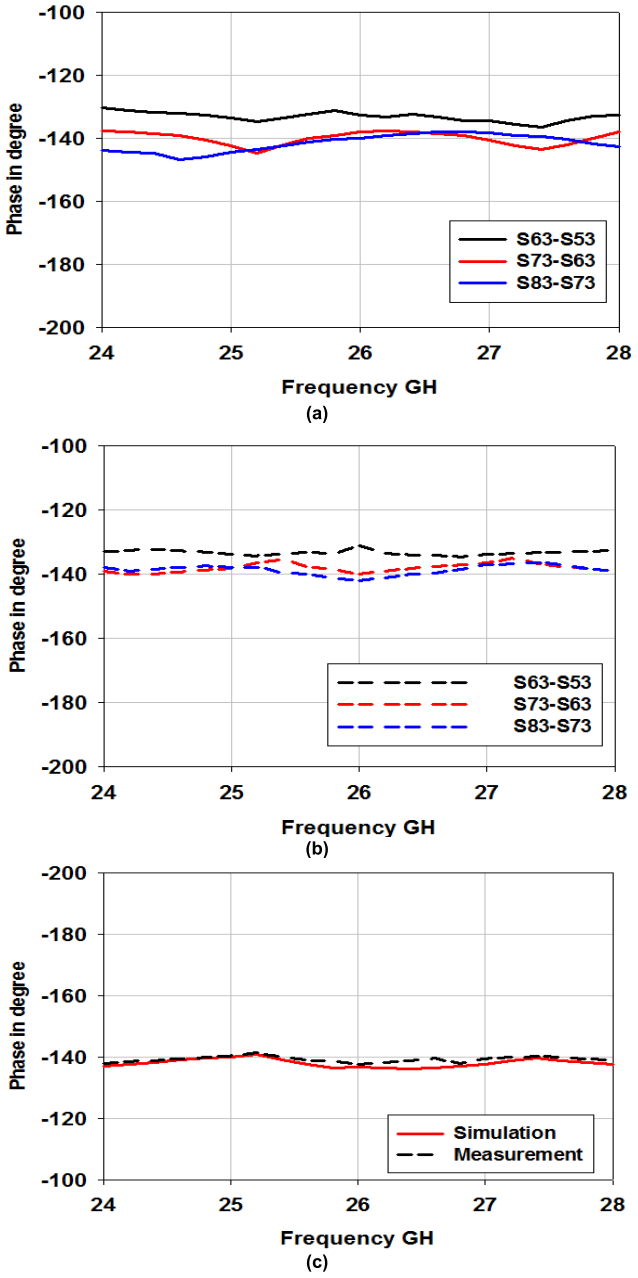

FIGURE 22. Phase shift at the output ports for the Port-3 excitation (a) Simulated, (b) Measured response, (c) Average phase differences.

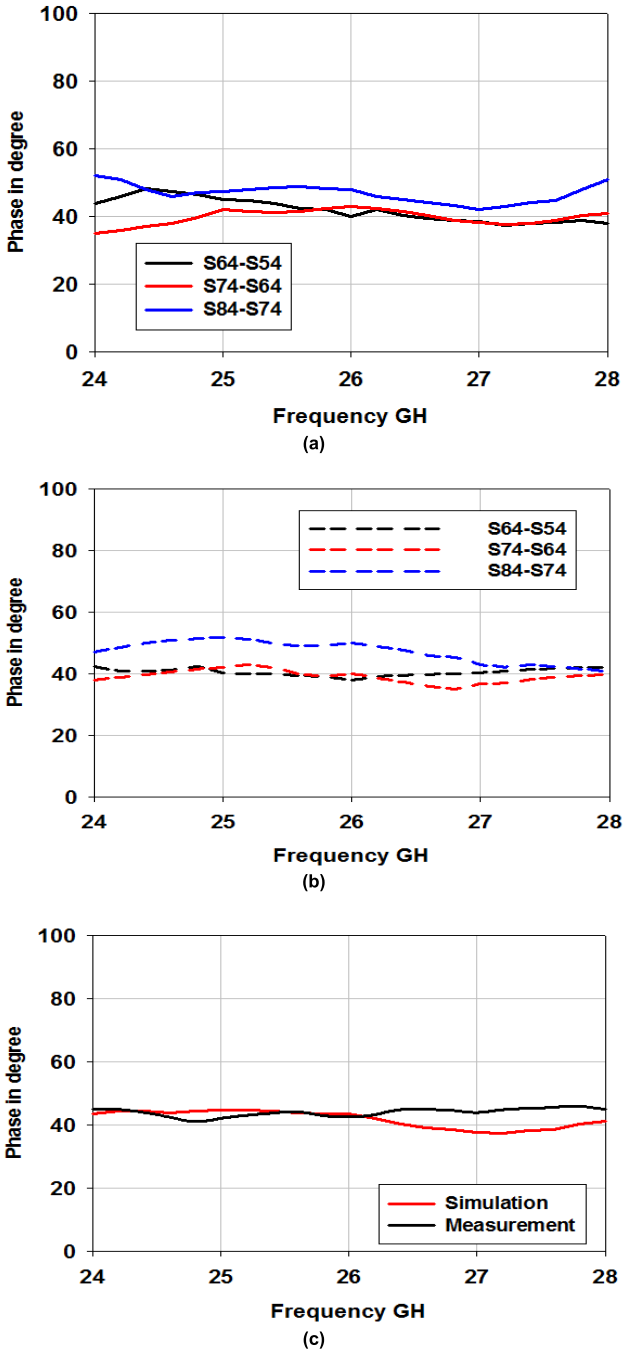

FIGURE 23. Phase shift at the output ports for the Port-4 excitation (a) Simulated, (b) Measured response, (c) Average phase differences.

at 26 GHz. The simulated phase difference values fluctuate from the target value of +45° by 5°, 2° and 3°, respectively. The average phase difference was 43,6° and phase error are 1.4 °.

For the excitation of Port-4, the measured phase differences achieved between the output ports are 38°, 40° and 50°, respectively, at 26 GHz. It is important to note here that from the measured phase difference values, the error is 3°, 5° and 5°, respectively, which led to an average phase difference was 42.6° and error of 2.4°. Table 4 illustrates a good agreement between the simulated and measured results of the phase difference between output ports.

B. ANTENNA BEAMFORMING RESULTS

The planar implementation of the linear antenna array with BM is performed by the combination of the designed SIW antenna and BM, at center frequency 26 GHz. BFN with microstrip straight feedline has been fabricated as seen in Figure 24 and tried to solder SMA but all in vain because the distance between each adjacent port was not enough. figure 25 presents the fabrication of BFN with a microstrip separation feedline. SIW butler matrix,

TABLE 4. simulated and measured results of phase difference between output ports.

Input port	Phase difference between output ports	Summation		Measurement	
		Phase (deg)	Average phase	Phase (deg)	Average phase
P1	Phase (S61-S51)	-47.7	-43.9	-50	-42.9
	Phase (S71-S61)	-41		-40	
	Phase (S81-S71)	-43		-41	
P2	Phase (S62-S52)	138	135.66	140	136.33
	Phase (S72-S62)	137		139	
	Phase (S82-S72)	132		130	
P3	Phase (S63-S53)	-132.5	-136.83	-131	-137.667
	Phase (S73-S63)	-138		-140	
	Phase (S83-S73)	-140		-142	
P4	Phase (S64-S54)	40	43.6	38	42.6
	Phase (S74-S64)	43		40	
	Phase (S84-S74)	48		50	

SIW array antenna, and microstrip separation feedline fabricated on the single ground plane and used roger substrate with thickness 0.508mm. The measurement of the BFN was made after the fabrication process was completed. By evaluating the phase and magnitude of the incident and reflected waves from a device under test (DUT), the VNA can accurately measure the linear behavior of the DUT. reflection coefficient, VNA is used for performing any measurement, it must be calibrated. Ordinarily, the calibration process moves the VNA measurement reference plane to the very ends of the test cables. The location of the reference plane is one factor that affects VNA measurement.

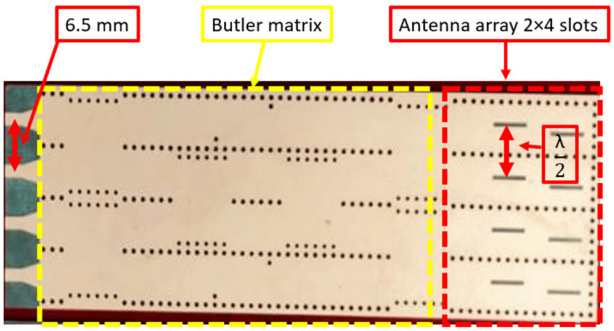

FIGURE 24. BFN with microstrip straight feedline.

Figure 26 presented the S parameters of BFN at all input ports, port1 is S11 = −21dB, port2 is S22 = −15, port3 is S33 = −20dB and port4 = −22dB. All input ports below −10dB with wider bandwidth 4GHz at resonate frequency 26GHz. This meant that the beamforming feeding network performs well at desired bandwidth. However, at port 2 and port 3 a rubble in the signal was noticed due to mismatch between connectors and ports as well as cable losses.

Figure 27 (a-b-c-d) shows the simulated and measured results of the radiation pattern of linear 1 × 4 antenna array with a spacing of 0.5λ, when Port-1, Port-2, Port-3 and Port-4 of the BFN are excited. The simulation results

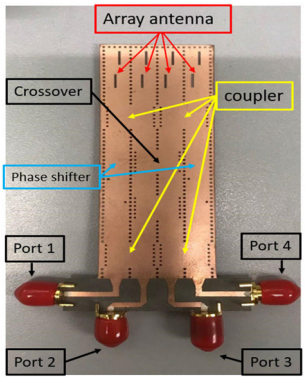

FIGURE 25. The fabricated prototype of the proposed four-beam antenna.

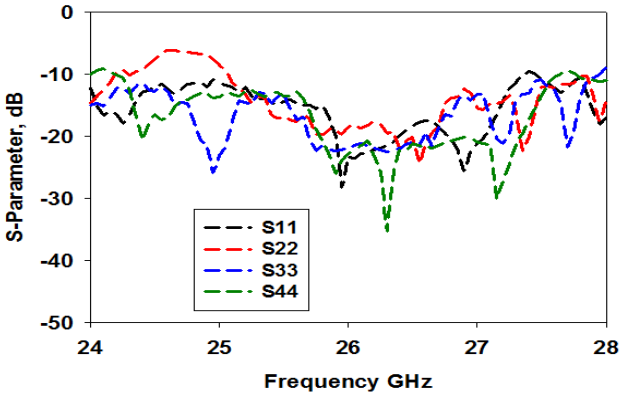

FIGURE 26. The measured return loss at all input ports of the printed beamforming network.

were already discussed in the previous section, so now onwards, the discussion is related to the measured results. When Ports-1 or 4 were excited, a gain of 10.7 dB and 10.4 dB was achieved, respectively. Meanwhile, the gain was 11.5 dB and 10.1 dB for Port-2 and Port-3 excitation, respectively. However, according to which input was excited, the peak of the beam rotates.

When Port-1 was fed with a signal, the main beam steered to −14°. Meanwhile, the direction of maximum radiation was attained at −41°, as the signal was fed into Port-2, for the Port-3 excitation, the main beam steers to +40°. When Port-4 was excited, the direction of main beam alters to +14°. Figure 27 show Simulated and measured radiation patterns of the multi beam antenna array. the radiation pattern measurement which done in the Anechoic Chamber of Advanced Microwave and RF Antenna Lab, Universiti Teknologi Malaysia (UTM), Johor, Malaysia. The tested antennas placed towards the source antenna as shown in Figure 28. As a conclusion, low phase error of 5° at port 2 is achieved as can see in table 5. Table 6 compares the performance of the proposed Butler matrix prototype with other related designs. It can be concluded from the comparison that the prototype has a low phase error.

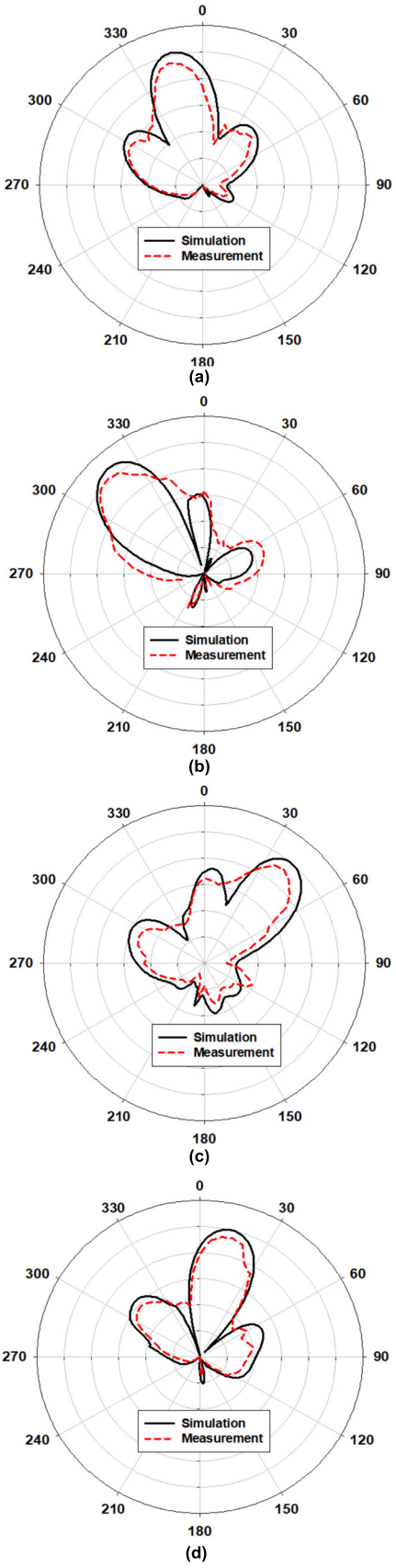

FIGURE 27. The performance of measured and simulated of radiation pattern of the proposed antenna beamforming. (a) Port 1. (b) Port 2. (c) Port 3. (d) Port 4.

TABLE 5. Radiation beam of beamforming.

Number of Port	Perfect Phase	Simulation		Measurement	
		Phase beam	Phase Error	Phase beam	Phase Error
1	-15	-14	1	-14	1
2	-45	-42	3	-41	4
3	+45	+41	4	+40	5
4	+15	+14	1	+14	1

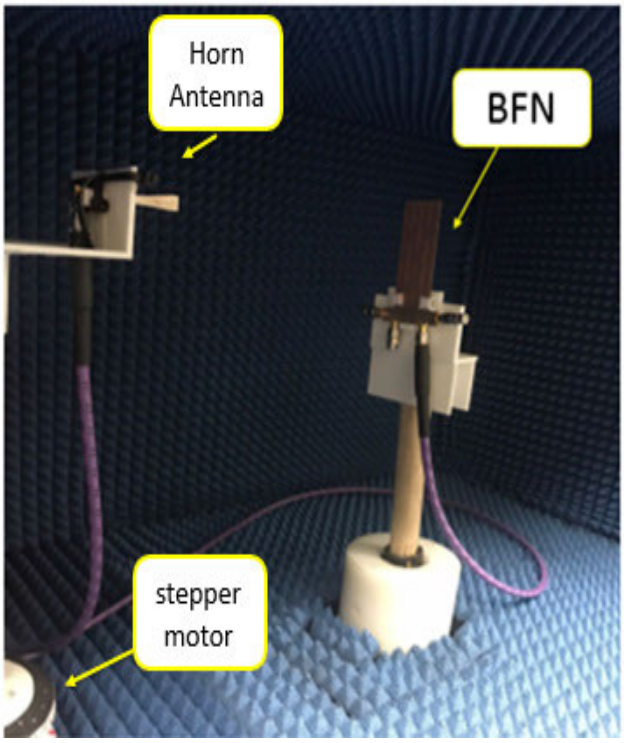

FIGURE 28. The proposed design SIW beamforming during measure radiation pattern.

TABLE 6. Compression with related work.

Parameters	[14]	[24]	[25]	[26]	This work
Frequency (GHz)	30	30	28	28	26
Return loss (dB)	22	28	27	18	22
Coupling factor (dB)	7 to 8	7 to 8	8 to 9	6 to 7	6 to 7
Coupling losses (dB)	3	3	4	0.65	1.68
Phase difference (deg)	±50, ±129	±50, ±129	±24, ±120	±42, ±133	±46, ±133
Phase errors (deg)	13	7	15	4	2
Technology	SIW	SIW	SIW	Waveguide cavity	SIW
Beamformer	4 × 4 BM	4 × 4 BM	4 × 4 BM	4 × 4 BM	4 × 4 BM

IV. CONCLUSION

In this paper, a low loss wideband of a 4 × 4 beamforming Butler Matrix at 26 GHz for 5G base station

application is presented to generate a unique four progressive phase difference at the output ports. The design of 4 × 4 Butler matrix has four hybrid couplers, one crossover, and two-phase shifters that achieved significant size reduction. Measurement results and simulation results agree well with each other to validate the design specifications. A low loss magnitude error of 3 dB and phase error of 5° with wideband of 4 GHz are achieved. Then, the proposed Butler matrix is attached with four SIW slot antennas to prove the property of a unique beam scanning. The measured results approve the concept of the four different phase scanning's at −14°, −41°, 40°, and −14° with a return loss below −10 dB. For 26 GHz fifth generation applications, the proposed 4 × 4 antenna Butler matrix has a new approach for beamforming network designs with the achieved characteristics.

REFERENCES

[1] L. Li, D. Wang, X. Niu, Y. Chai, L. Chen, L. He, X. Wu, F. Zheng, T. Cui, and X. You, "mmWave communications for 5G: Implementation challenges and advances," *Sci. China Inf. Sci.*, vol. 61, no. 2, pp. 1–19, Feb. 2018, doi: 10.1007/s11432-017-9262-8.

[2] W. Choi, K. Park, Y. Kim, K. Kim, and Y. Kwon, "A *V*-band switched beam-forming antenna module using absorptive switch integrated with 4 × 4 Butler matrix in 0.13-μm CMOS," *IEEE Trans. Microw. Theory Techn.*, vol. 58, no. 12, pp. 4052–4059, Dec. 2010, doi: 10.1109/TMTT.2010.2086472.

[3] F. Casini, R. V. Gatti, L. Marcaccioli, and R. Sorrentino, "A novel design method for Blass matrix beam-forming networks," in *Proc. Eur. Radar Conf.*, Oct. 2007, pp. 232–235, doi: 10.1109/EURAD.2007.4404979.

[4] Y. J. Cheng, W. Hong, K. Wu, Z. Q. Kuai, C. Yu, J. X. Chen, J. Y. Zhou, and H. J. Tang, "Substrate integrated waveguide (SIW) Rotman lens and its Ka-band multibeam array antenna applications," *IEEE Trans. Antennas Propag.*, vol. 56, no. 8, pp. 2504–2513, Aug. 2008, doi: 10.1109/TAP.2008.927567.

[5] S.-G. Mok, C.-W. Jung, S.-J. Ha, and Y. Kim, "Switchable beam pattern antenna for wireless communication devices," in *Proc. IEEE Int. Symp. Antennas Propag. (APSURSI)*, Jul. 2011, pp. 1308–1310, doi: 10.1109/APS.2011.5996529.

[6] C. Liu, S. Xiao, Y.-X. Guo, M.-C. Tang, Y.-Y. Bai, and B.-Z. Wang, "Circularly polarized beam-steering antenna array with Butler matrix network," *IEEE Antennas Wireless Propag. Lett.*, vol. 10, pp. 1278–1281, 2011, doi: 10.1109/LAWP.2011.2176903.

[7] C. Dall'Omo, T. Monediere, B. Jecko, F. Lamour, I. Wolk, and M. Elkael, "Design and realization of a 4 × 4 microstrip Butler matrix without any crossing in millimeter waves," *Microw. Opt. Technol. Lett.*, vol. 38, no. 6, pp. 462–465, Sep. 2003, doi: 10.1002/mop.11090.

[8] A. B. Guntupalli, T. Djerafi, and K. Wu, "Two-dimensional scanning antenna array driven by integrated waveguide phase shifter," *IEEE Trans. Antennas Propag.*, vol. 62, no. 3, pp. 1117–1124, Mar. 2014, doi: 10.1109/TAP.2013.2292935.

[9] W. Hong, Z. H. Jiang, C. Yu, J. Zhou, P. Chen, Z. Yu, H. Zhang, B. Yang, X. Pang, M. Jiang, Y. Cheng, M. K. T. Al-Nuaimi, Y. Zhang, J. Chen, and S. He, "Multibeam antenna technologies for 5G wireless communications," *IEEE Trans. Antennas Propag.*, vol. 65, no. 12, pp. 6231–6249, Dec. 2017, doi: 10.1109/TAP.2017.2712819.

[10] J.-W. Lian, Y.-L. Ban, C. Xiao, and Z.-F. Yu, "Compact substrate-integrated 4 × 8 Butler matrix with sidelobe suppression for millimeter-wave multibeam application," *IEEE Antennas Wireless Propag. Lett.*, vol. 17, no. 5, pp. 928–932, May 2018, doi: 10.1109/LAWP.2018.2825367.

[11] J.-W. Lian, Y.-L. Ban, Q.-L. Yang, B. Fu, Z.-F. Yu, and L.-K. Sun, "Planar millimeter-wave 2-D beam-scanning multibeam array antenna fed by compact SIW beam-forming network," *IEEE Trans. Antennas Propag.*, vol. 66, no. 3, pp. 1299–1310, Mar. 2018, doi: 10.1109/TAP.2018.2797873.

[12] J.-W. Lian, Y.-L. Ban, Z. Chen, B. Fu, and C. Xiao, "SIW folded Cassegrain lens for millimeter-wave multibeam application," *IEEE Antennas Wireless Propag. Lett.*, vol. 17, no. 4, pp. 583–586, Apr. 2018, doi: 10.1109/LAWP.2018.2804923.

[13] S. Karamzadeh, V. Rafii, M. Kartal, and B. S. Virdee, "Compact and broadband 4 × 4 SIW Butler matrix with phase and magnitude error reduction," *IEEE Microw. Wireless Compon. Lett.*, vol. 25, no. 12, pp. 772–774, Dec. 2015, doi: 10.1109/LMWC.2015.2496785.

[14] Q.-L. Yang, Y.-L. Ban, J.-W. Lian, Z.-F. Yu, and B. Wu, "SIW Butler matrix with modified hybrid coupler for slot antenna array," *IEEE Access*, vol. 4, pp. 9561–9569, 2016, doi: 10.1109/ACCESS.2016.2645938.

[15] S. Kumari and S. Srivastava, "Losses in waveguide and substrate integrated waveguide (SIW) for Ku band: A comparison," *Int. J. Mod. Eng. Res.*, vol. 3, no. 1, pp. 53–57, 2013.

[16] L. Cao, A.-S. Grimault-Jacquin, and F. Aniel, "Comparison and optimization of dispersion, and losses of planar waveguides on benzocyclobutene (BCB) at THz frequencies: Coplanar waveguide (CPW), Microstrip, stripline and slotline," *Prog. Electromagn. Res. B*, vol. 56, pp. 161–183, 2013, doi: 10.2528/PIERB13072603.

[17] M. W. Sabri, N. A. Murad, and M. K. A. Rahim, "Highly directive 3D-printed dual-beam waveguide slotted antennas for millimeter-wave applications," *Microw. Opt. Technol. Lett.*, vol. 61, no. 6, pp. 1566–1573, Jun. 2019, doi: 10.1002/mop.31834.

[18] M. J. Tavakoli and A. R. Mallahzadeh, "Wideband directional coupler for millimeter wave application based on substrate integrated waveguide," *Emerg. Sci. J.*, vol. 2, no. 2, pp. 93–99, May 2018, doi: 10.28991/esj-2018-01132.

[19] K. B. Kumar and T. Shanmuganantham, "SIW hydride coupler for mm-wave applications," in *Proc. Int. Conf. Control, Instrum., Commun. Comput. Technol. (ICCICCT)*, Dec. 2016, pp. 246–250, doi: 10.1109/ICCICCT.2016.7987953.

[20] B. W. Xu, S. Y. Zheng, Y. M. Pan, and Y. H. Huang, "A universal reference line-based differential phase shifter structure with simple design formulas," *IEEE Trans. Compon., Packag., Manuf. Technol.*, vol. 7, no. 1, pp. 123–130, Jan. 2017, doi: 10.1109/TCPMT.2016.2633483.

[21] H. Peng, P. Jiang, T. Yang, and H. Jin, "Continuously tunable SIW phase shifter based on the buried varactors," *IEICE Electron. Express*, vol. 12, no. 7, 2015, Art. no. 20150165, doi: 10.1587/elex.12.20150165.

[22] S. Moitra, A. K. Mukhopadhyay, A. K. Bhattacharjee, and A. K. Bhattacharjee, "Ku-band substrate integrated waveguide (SIW) slot array antenna for next generation networks," *Global J. Comput. Sci. Technol. Netw., Web Secur.*, vol. 13, no. 5, pp. 1–7, 2013.

[23] [Online]. Available: https://www.microwavejournal.com/articles/37280-a-survey-of-substrate-integrated-waveguide-bandpass-filter-development

[24] M. M. Pezhman, A.-A. Heidari, and A. Ghafoorzadeh-Yazdi, "A compact 4 × 4 SIW beamforming network for 5G applications," *AEU Int. J. Electron. Commun.*, vol. 135, Jun. 2021, Art. no. 153714, doi: 10.1016/j.aeue.2021.153714.

[25] M. K. Khattak, S. Kahng, M. S. Khattak, A. Rehman, C. Lee, and D. Han, "A low profile, wideband and high gain beam-steering antenna for 5G mobile communication," in *Proc. IEEE Int. Symp. Antennas Propag. USNC/URSI Nat. Radio Sci. Meeting*, Jul. 2017, pp. 2575–2576, doi: 10.1109/APUSNCURSINRSM.2017.8073330.

[26] *3D Printed Waveguide-Based Butler Matrix Antenna Beamforming for Millimeterwave Applications Muataz Watheq Sabri Almeshehe Universiti Teknologi Malaysia Declaration of Thesis/Undergraduate Project Report and.*

YAQDHAN MAHMOOD HUSSEIN was born in Samawah, Iraq, in 1991. He received the B.S. degree in computer technology engineering from Islamic University College, Najaf, Iraq, in 2015, the M.S. degree in electronic engineering (telecommunication systems) from Universiti Teknikal Malaysia Melaka (UTeM), Malaysia, in 2018, and the Ph.D. degree in electronic engineering from Universiti Teknologi Malaysia (UTM), Johor Bahru. His current research interests include millimeter wave antennas, base station antennas, and SIW technology with Butler matrix.

MOHAMAD KAMAL A. RAHIM (Senior Member, IEEE) was born in Alor Setar, Kedah, Malaysia, in 1964. He received the B.Eng. degree in electrical and electronic engineering from the University of Strathclyde, U.K., in 1987, the master's degree in engineering from the University of New South Wales, Australia, in 1992, and the Ph.D. degree in wideband active antenna from the University of Birmingham, U.K., in 2003. From 1992 to 1999, he was a Lecturer with the Faculty of Electrical Engineering, Universiti Teknologi Malaysia (UTM), where he was a Senior Lecturer with the Department of Communication Engineering, from 2005 to 2007. He is currently a Professor with UTM. His research interests include the design of active and passive antennas, dielectric resonator antennas, microstrip antennas, reflectarray antennas, electromagnetic bandgaps, artificial magnetic conductors, left-handed metamaterials, and computer-aided design for antennas.

NOOR ASNIZA MURAD (Senior Member, IEEE) received the B.E. degree in electrical and telecommunications engineering, and the M.E. degree in electrical engineering from Universiti Teknologi Malaysia (UTM), in 2001 and 2003, respectively, and the Ph.D. degree from the Emerging Device Technology Group, University of Birmingham, U.K., in 2011, with a focus on micromachined millimeter-wave circuits. Shortly after graduation, she was a Tutor with UTM, where she was appointed as a Lecturer in April 2003. She is currently an Associate Professor with the Faculty of Electrical Engineering, Universiti Teknologi Malaysia (UTM). She was attached to HID GLOBAL Sdn Bhd, for one year, under research and development specifically working on RFID tag design, testing, and development. Her research interests include antenna design for RF, microwave, and millimeter wave communication systems, RFID, metamaterials, and antenna beamforming circuits.

HATEM ODAY HANOOSH was born in Samawah, Iraq, in 1991. He received the B.S. degree in computer technology engineering from Islamic University College, Najaf, in 2015, the M.S. degree in electronic engineering (telecommunication systems) from Universiti Teknikal Malaysia Melaka (UTeM), Malaysia, in 2018, and the Ph.D. degree in electronic engineering from Universiti Teknologi Malaysia (UTM), Johor Bahru. His current research interests include millimeter-wave antennas, base station antennas, and waveguide slot antennas.